UC San Diego

UC San Diego Previously Published Works

Title

Densely distributed and real-time scour hole monitoring using piezoelectric rod sensors

Permalink

https://escholarship.org/uc/item/1sm042vm

Journal

Advances in Structural Engineering, 22(16)

ISSN

1369-4332

Authors

Funderburk, Morgan L
Huang, Shieh-Kung
Loh, Chin-Hsiung
et al.

Publication Date

2019-12-01

DOI

10.1177/1369433219831124

Peer reviewed

eScholarship.org Powered by the California Digital Library
University of California

Research Paper

*Corresponding Author:

Kenneth J. Loh, University of California-San Diego, Department of Structural Engineering, 9500 Gilman Dr, MC 0085, La Jolla, CA 92093-0085, USA.

Email: kenloh@ucsd.edu

Densely Distributed and Real-time Scour Hole Monitoring using Piezoelectric Rod Sensors

Morgan Funderburk[1], Shieh-Kung Huang[1,2], Chin-Hsiung Loh[1,2], and Kenneth J. Loh[1,*]

[1]Department of Structural Engineering, University of California-San Diego, La Jolla, CA
[2]Department of Civil Engineering, National Taiwan University, Taipei, Taiwan

Abstract

This study aims to validate a piezoelectric driven-rod scour monitoring system that could sense changes in scour depth along the entire rod at its instrumented location. The proposed sensor is a polymeric slender rod with a thin strip of polyvinylidene fluoride that runs through its midline. Extraction of the fundamental frequency allows the direct calculation of the exposed length (or scour depth) of the slender rod undergoing fluid flow excitation. First, laboratory validation in dry conditions is presented. Second, hydrodynamic testing of the sensor system in a soil-bed flume is discussed. Each rod was installed using a 3D-printed footing designed for ease of installation and stabilization during testing. The sensors were installed in a layout designed to capture symmetric scour conditions around a scaled pier. In order to analyze the system out of steady-state conditions, water velocity was increased in stages during testing to induce different degrees of scour. As ambient water flow excited the portion of the exposed rods, the embedded piezoelectric element outputted a time-varying voltage signal. Different methods were then employed to extract the fundamental frequency of each rod, and the results were compared. Further testing was also performed to characterize the relationship between frequency outputs and flow velocity, which were previously thought to be independent. In general, the proposed driven-rod scour monitoring system successfully captured changing frequencies under varied flow conditions.

Keywords

Flume testing, frequency analysis, passive sensing, piezoelectric, vibration, scour monitoring, structural health monitoring

Introduction

Over 200 bridges collapsed in the U.S. between 1992 and 2014 due to a hydraulic-induced failure, including local scour (Montalvo & Cook 2017). Local scour is a complex phenomenon that is not well-predicted in lab experiments and is exceptionally hard to measure in the field (U.S. Department of Transportation 2005). Although there are different mechanisms in which scour occurs, local scour refers particularly to sediment erosion around obstructions in flow, typically a bridge pier or abutment (Melville 1975) (Fig. 1). Sediment removal around the foundation undercuts structural stability of the pier, putting the entire superstructure at risk (Stein et al. 1999). Many factors affect the severity of scour including the bed sediment cohesiveness, flow dynamics, and river geometry (Richardson 1989). However, the U.S. Department of Transportation (2005) reports that, in most field cases, these factors are not or cannot be well documented. Fluctuating river conditions can mask extreme scour events, where deep holes are replaced with poorly compacted soil. Even if the superstructure does not fail during an extreme flow event, the structure will suffer from a compromised foundational system that appears unharmed (Richardson 1989; U.S. Department of Transportation 2009). The complexity of local scour necessitates the development of continuous monitoring systems for evaluating the extent of scour and for further understanding local scour phenomenon.

Currently, the Federal Highway Administration (FHWA) recommends scour-monitoring techniques that fall into two categories: portable and fixed systems (U.S. Department of Transportation 2009). Portable systems are typically used due to cost effectiveness but will always miss periods of scour-and-infill, where sediments are removed during a high flow period but settles back after flow normalizes (Hunt 2009). On the other hand, fixed sensors offer more frequent or constant monitoring that may be

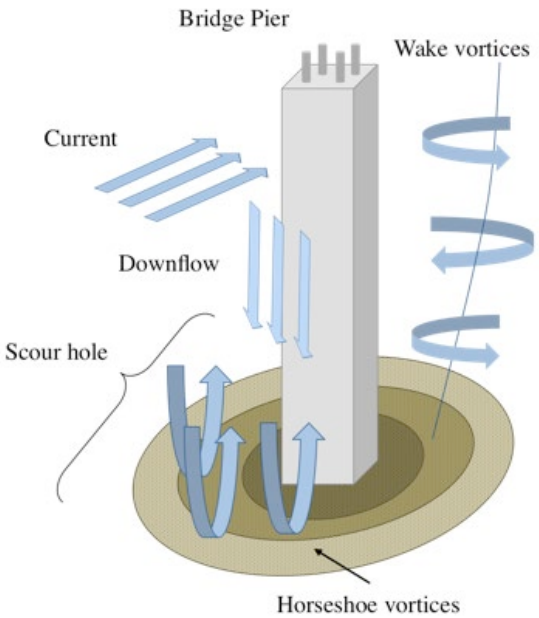

Figure 1. The illustration depicts the flow conditions present during scour. The current undergoes downflow once reaching the face of the pier. After the initial formation of the scour hole, horseshoe vortices form and magnify, thereby deepening of the hole upstream. Turbulent wake vortices displace sediments downstream.

more likely to detect critical scour events. Examples of fixed sensors include sonar devices, magnetic sliding collars, tilt sensors, float out devices, sounding rods, and time domain reflectometers (TDRs). Fixed sonar devices typically only offer selective discrete data but can monitor these points constantly in order to develop time histories (De Falco & Mele 2002). However, these devices suffer from operating only in ideal water conditions, where sound waves can easily propagate. Magnetic sliding collars only detect maximum scour depth and are suitable for piers with circular cross-sections (Richardson, Richardson & Lagasse, 1996). Tilt sensors detect changes in the bridge superstructure but are influenced by normal bridge movement unrelated to scour (U.S. Department of Transportation 2009; Yao et al. 2010). Float out devices must be reset after each event and are limited by their battery life (Yao et al. 2010). Sounding rods are susceptible to streambed penetration in sand bed applications and may induce scour around their base (Hunt 2009; Lagasse et al. 1991). TDRs offer continuous data undisturbed by water conditions but have limits on their maximum length for signal reliability (U.S. Department of Transportation 2009; Yankielun & Zabilansky 1999). Based on these aforementioned limitations, it is clear that more effective scour monitoring techniques are still direly needed.

Many interesting solutions for scour monitoring have been proposed in recent years, all aimed at finding more accurate and substantial information on local scour and its effects on bridges. Some of these new types of sensors generally fall into three categories: (1) "smart rocks"; (2) vibration-based structural scour monitoring; and (3) buried "stack" or "rod" sensors. First, smart rocks are small magnets embedded in acrylic balls whose positions are detected using magnetic field interference. The locations are determined in relation to an anchored "master rock" at the base of the pier (Chen et al. 2015). Smart rocks are unique due to their lack of anchoring to the pier or surrounding environment; however, they can be washed away during severe flow events. Vibration-based monitoring, using either ambient or forced excitations, utilizes changes in detected structural properties to infer scour-induced damage (Bao & Liu 2017). However, structural damage and environmental effects also affect these same structural properties, so deducing scour damage may prove difficult.

In fact, the largest class of new sensors consists of buried "stack" or "rod" sensors. These transducers are based on erosion exposing different portions of a sensor over time, either along a sensing rod or simply installed in a stack on the pier itself. The types of stack/rod sensors include fiber Bragg grating (FBG) buttons (Lin et al. 2005), FBG coupled with water-swellable polymers (Kong et al. 2017), dissolved oxygen (DO) sensors (Azhari et al. 2015), accelerometer stacks (Chen et al. 2016), and discrete piezoelectric film sensors (Wang et al. 2012). Many of these sensors can only be installed in close proximity to the pier due to power and wiring constraints. FBG sensors are costly, sensitive to temperature, and require interrogation to collect data. While these transducers provide real-time feedback on scour depth, all of them offer only discrete measurement points; this means that scour measurements could only be obtained at discrete depths along the stack where the sensors are instrumented, not to mention that a large number of sensors are needed in each stack and at every location. Of final note is the development of an FBG vibration-based rods that uses feedback from the strain sensor to detect frequency, from which length of the exposed rod (*i.e.*, scour depth) can

be back-calculated (Zarafshan et al. 2011). This FBG sensor uses the same structural mechanism discussed in this study. However, this sensor also suffers from the locational, environmental, interrogation, and cost constraints associated with FBGs.

Previous iterations of a slender piezoelectric polyvinylidene fluoride (PVDF) thin film encased in a flexible rod (piezo-rod), which mitigate drawbacks from the existing and emerging technologies, were developed for scour monitoring (Azhari & Loh 2017). The piezo-rods could be buried systematically in locations surrounding a bridge pier. The electromechanical properties of PVDF allow these types of sensors to output voltage time histories when subjected to hydrodynamic excitations from flowing water. The voltage time history data are then acquired, processed, and analyzed for its instantaneous fundamental frequency of vibration, whereby the length of the piezo-rod (*i.e.*, scour depth or exposed length of the rod) could be directly calculated. Using a network of these sensors, sediment depth at different locations could be plotted spatially to produce a scour topography map. The passive nature of piezoelectric transducers is ideal for scour monitoring, since it generates a voltage in response to strain, thus eliminating the need for an external power source. Although the tests showed that the piezo-rods located on the sides of the pier generated good voltage response, a wide spread of identified frequencies was found in areas where sensors underwent less excitation. Thus, sensor optimization and improvements in data processing are needed, as well as demonstration of their potential for larger scale implementations.

Therefore, the objective of this study is to demonstrate that sensor design improvements and different signal processing techniques can enhance the quality of frequency data extracted. This paper begins with outlining the fabrication of an extendable PVDF sensor strip and the design of an appropriate footing system. Tests conducted in dry sand, followed by hydrodynamic scour testing, are discussed. Various signal-processing schemes are then employed to extract the frequency-domain features of the sensors for estimating scour depth. Finally, the relationship between flow velocities and sensor response is discussed.

Background

Sensing Mechanism

The scour sensor developed for this study is a thin strip of PVDF piezoelectric polymer film embedded in a slender, hollow, polymer rod. As mentioned earlier, the rod would be buried underneath the soil and, when exposed by scour, would undergo hydrodynamic excitation from ambient flowing water. The flow-induced vibrations of the piezo-rod would then output a voltage time history, owing to the PVDF film's piezoelectricity. The natural frequencies of the piezo-rod can be determined by solving the well-known differential equation describing a continuous beam undergoing free-vibration using the boundary conditions of a fixed-end cantilevered beam (Meirovitch 1967):

$$\frac{d^2}{dx^2}\left\{EI\frac{d^2y(x)}{dx^2}\right\} - \rho A y(x)\omega^2 = 0 \qquad (1)$$

where E is elastic modulus, I is moment of inertia, $y(x)$ is the deflection of the beam at location x along longitudinal axis of the beam or piezo-rod, ρ is density, A is cross-sectional area, and ω is angular frequency.

Wherein the fundamental frequency, f_n, is calculated to be:

$$f_n = \frac{1.876^2}{2\pi L^2}\sqrt{\frac{EI}{\rho A}} \tag{2}$$

where exposed length L is equivalent to a distance x from the free- to the fixed-end of the beam. Solving for L, this yields:

$$L = 1.876\left[\frac{EI}{\rho A(2\pi f_n)^2}\right]^{1/4} \tag{3}$$

As shown in Equation 2, frequency is inversely proportion to the square of the length. Therefore, the length of the cantilever exposed to excitation can be determined by analyzing the outputted voltage time history in the frequency domain. As sediment is removed from around the piezo-rod, its length will increase proportionally, which will alter the frequency content of its generated voltage time history (Fig. 2). The depth of scour can be determined by subtracting the initial rod length from its instantaneous length (or exposed length of the beam).

It should be noted that a cantilevered beam undergoing fluid excitation must consider the additional mass of exciting fluid (*i.e.*, water) (Chen et al. 1976). Since density is considered constant in the original differential equation, simply adding the density of water, ρ_w, to the sensor density, ρ_s, as part of Equation 2 enables one to estimate the cantilever's new natural frequency in water:

$$f_{nw} = \frac{1.876^2}{2\pi L^2}\sqrt{\frac{EI}{(\rho_s+\rho_w)A}} = \frac{f_n}{\sqrt{1+\rho_w/\rho_s}} \tag{4}$$

where f_n corresponds to natural frequency of the beam in vacuum. The added mass lowers the expected frequency output.

Signal Processing Methods

Digital filtering and frequency-domain analysis

Traditional frequency analysis was employed as the starting point of this study, as it was proven effective in previous validation tests (Azhari and Loh 2017). First, raw voltage data was smoothed using a moving average filter. Then the Chebyshev high-pass filter and a Butterworth low-pass filter were applied to remove frequencies outside of the range between 2 and 30 Hz. Furthermore, a Butterworth band-pass filter was applied to remove electric hum, which can sometimes be interpreted as a major frequency of sensor signals corresponding to low levels of excitation and low signal-to-noise ratio (Vaseghi 2008). After filtering, a fast Fourier Transform (FFT) was used to assess the prominent

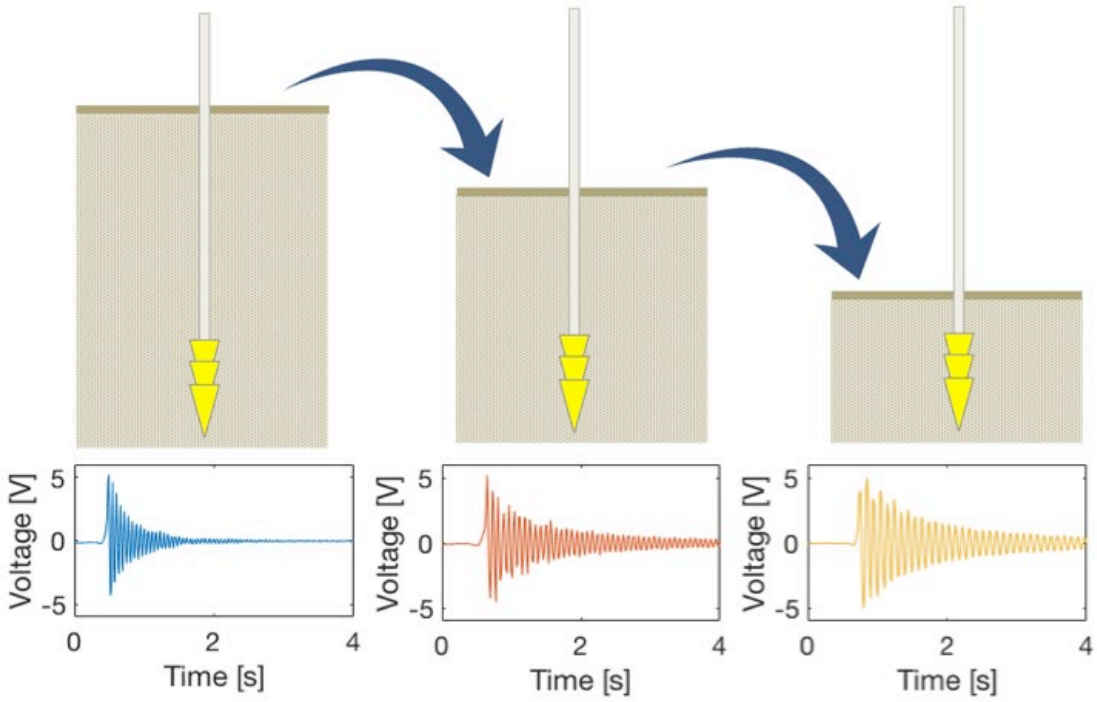

Figure 2. The illustration demonstrates the effect of scour on the piezo-rod's exposed length and subsequent output. As sediment erodes from around the sensor, the exposed length increases and is subject to vibrations. The voltage outputs below show changing free-vibration time response at increasingly exposed sensor lengths.

frequencies associated with the signal. A peak-picking algorithm with thresholding was used on the upper envelope of the estimated auto power spectral density (PSD) function for identifying the first fundamental modal frequency. The upper envelope is a smooth curve outlining the upper extremes of the PSD, which allows the peak-picking function to return only major peaks instead of the substantial number of local peaks that occur within the PSD.

Wavelet packet transform and Hilbert transform

For comparison purposes, two different transforms to extract the major frequency from the collected signals were implemented in this study. First, wavelet packet transform (WPT) can be used to decompose the signals measured from the piezo-rods. Second, Hilbert transform (HT) can be applied to find the instantaneous phase within the decomposed signals. The major frequency can then be evaluated by performing polynomial regression on the phase of the analytic signal.

Wavelet packet transform

WPT is a technique that partitions the time-frequency plane and delivers a decomposition for further analysis. WPT was utilized in this study for noise reduction purposes. Discrete wavelet transform (DWT) and WPT are performed by passing the signals through low-pass and high-pass quadrature mirror filters. In DWT, only the

previous approximation coefficient is passed through the filters to decompose each level, which returns both a new approximation and detail coefficient:

$$A_{j-1} = A_j + D_j \tag{5}$$

where A_j and D_j are the approximation and detail coefficients in level j, respectively. However, in WPT, both the detail and approximation coefficients are decomposed to create the full binary tree. WPT was selected because it outputs a selection of narrowband signal components that fall within a certain frequency range. Each of the WPT components comes with an equal bandwidth of $f_s/2^j+1$, where f_s is the sampling rate of the signal. After rearrangement using Paley (natural) ordering (Wickerhauser 1996), the central frequency of the i^{th} component function, $F_{c,i}$, can be expressed as:

$$F_{c,i} = \frac{(2i-1)f_s}{2^{j+2}} \tag{6}$$

where the leftmost component corresponds to the lowest frequency band at each level. A component corresponding to the desired frequency range is then selected as the smoothed voltage time history. WPT is advantageous for processing discretely sampled piezo-rod voltage time history, as signals are naturally analyzed within a tailorable frequency band with respect to time.

Hilbert transform

Once the signal was smoothed using WPT, Hilbert transform was employed to determine the instantaneous fundamental frequency. HT can be represented as a specific operator that produces a harmonic conjugate of a real function, $x(t)$. It is defined as an improper integral:

$$H[x(t)] = \frac{1}{\pi}\int_{-\infty}^{\infty} \frac{x(\tau)}{t-\tau}\, d\tau \tag{7}$$

In this case, the function $x(t)$ corresponds to the voltage time history of an individual sensor. HT also has a very simple interpretation in that it brings a 90° phase shift in the frequency domain. Consequently, the real and imaginary functions of $H[x(t)]$ correspond to each other in a unique way to create an analytic function (Johansson 1999):

$$z(t) = x(t) + iH[x(t)] = a(t)e^{i\phi(t)} \tag{8}$$

where $a(t)$ and $\phi(t)$ are amplitude and phase functions, respectively. If the signals closely approach a narrowband condition, the imaginary function will be in quadrature to the real function, and the analytic signals will approximate well. On the other hand, this transform will not be able to distinguish the amplitude and phase functions once the spectra of the signals are spread in the frequency domain.

For a continuous-time signal, the instantaneous frequency is obtained by computing (Van der Pol 1946):

$$f(t) = \frac{1}{2\pi}\frac{d\phi(t)}{dt} \quad (9)$$

For a discrete-time signal, the instantaneous frequency can be estimated by directly discretizing Equation (9) (Boashash 1992; Boashash & Jones 1992). The major frequency can then be obtained based on polynomial phase modeling with order p (Boashash et al. 1990):

$$\phi(t) = c_0 + c_1 t + c_2 t^2 + \cdots + c_P t^P \quad (10)$$

where c_0, c_1, c_2, …, c_p are constants. In this study, to simplify the frequency estimation process, order 1 was exploited, and the major frequency was derived by scaling c_1 by $1/2\pi$. In this case, the major frequency corresponds to the fundamental frequency of the piezo-rod sensor. The instantaneous fundamental frequency was then averaged within time windows corresponding to those used in the windowed FFT technique.

Experimental Details

Sensor Development

The shortfalls of the previous design of the piezo-rod system developed by Azhari and Loh (2017) were the delicacy of the base where the lead wires were housed and the limitation of sensor lengths (to only 280 mm). In order to demonstrate that this technology is a viable option for full-scale scour monitoring, the PVDF sensing element needed to be tailorable to a variety of lengths. Furthermore, this study investigated more sophisticated signal processing methods (versus FFT analysis) for extracting the piezo-rod's instantaneous natural frequency (*i.e.*, equivalent to exposed length or scour depth) during hydrodynamic excitations.

Extension of PVDF piezoelectric strip

Metallized Piezo Film Sheets with silver ink electrodes were purchased from Measurement Specialties Inc. The manufactured sheet was 110 µm thick, 280 mm long, and 203 mm wide. The sheets were cut lengthwise into 4 mm wide strips using a guillotine paper cutter. Leads were attached using 24 American Wire Gauge (AWG) multi-strand wire soldered to copper tape. The connection was further reinforced using colloidal silver paste (Ted Pella). The extension of the PVDF strip was done in accordance to the lead connection, which was shown to be effective. To prevent contact between the metallic faces, a double-sided acetate tape was used to connect two 4 mm strips end-to-end. Then, copper tape and silver paint were used to form a connection between the two films that now lay on the same plane (Fig. 3). To produce the maximum length shown in this study, this process was repeated twice, forming a 4 mm strip with a length of ~ 900 mm. The extension process was performed in a similar manner to produce the 350 mm long sensor used during flume testing.

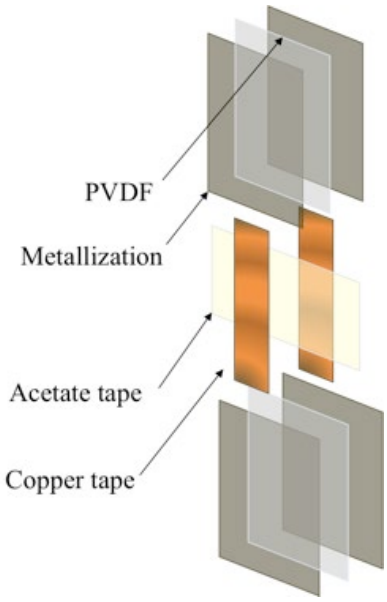

Figure 3. Individual PVDF strips are connected to one another using copper tape to extend their lengths.

Driven-rod sensor design and fabrication

In this study, the piezo-rods were redesigned to incorporate materials suitable for long-term water exposure (Azhari & Loh 2017). The cross-section of the sensor is illustrated in Figure 4a. First, the outer structure of the piezo-rods was a 6 mm diameter polypropylene hollow cylinder that was temporarily capped at one end. Second, TAP Plastics Fast-Hardening Marine Grade Epoxy System was mixed at a 4:1 base to curing agent ratio. The mixture was rigorously shaken for ~ 1 min or until the mixture appeared to be fully homogenous and then transferred into the cylinder. Third, a PVDF strip was then affixed to an acrylic rod with a 3 mm diameter. Then, the acrylic rod with the PVDF film was then carefully inserted into the polypropylene hollow rod until the entire sensor was submerged in epoxy while ensuring that there was enough epoxy in the capped end to form a watertight plug. The sensors were then allowed to cure inside a fume hood overnight in an upright position.

In this study, a new footing system was developed and prototyped by 3D printing polylactic acid (PLA) cone tips (Fig. 4b). The cone tip features a stair-step face designed for being driven into soil, as one would do when driving piles into the ground. The stepped face is purposefully designed to add stability and rigidity so that sensors cannot be pulled out or displaced from the soil easily. Numerous cone halves were printed simultaneously and then bonded together using a quick-drying epoxy to obtain 10 cone tips in each batch. In larger scale implementations, these cones can be machined from metal alloys. It should be mentioned that two holes were included during printing of the cone, namely, one at the top to hold the base of the sensor and another on the side to accommodate the lead wires of the piezo-rods. Then, the lead wires were threaded through the side hole, followed by filling the top hole with quick-drying epoxy. The sensor was then press-fitted into the top hole, allowing the epoxy to form a complete seal around the base of the sensor and the protruding wires (Fig. 4b). Finally, each piezo-rod

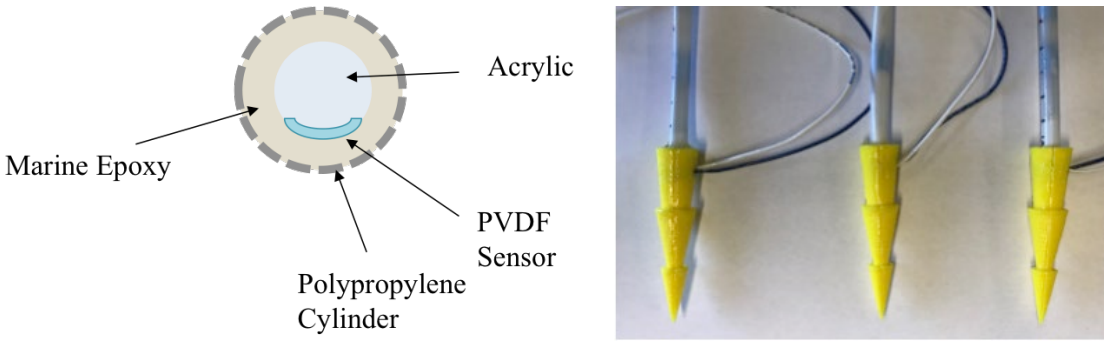

Figure 4. (a) The cross-section of the piezo-rod shows that the PVDF strip is embedded in the polypropylene cylinder and encased in marine epoxy. (b) Driven cone footings optimized for 3D batch printing were fabricated, fitted onto the base of the piezo-rod, and sealed with epoxy to prevent water infiltration.

was also marked every centimeter along its length so that their exposed length could be determined visually during testing.

Free-vibration testing with fixed support

To validate the performance and quality of measurements of the lengthened PVDF strip (*i.e.*, up to ~ 1 m long), a cantilevered beam test setup was employed. The test structure was a 1.2 m long, 0.1 m wide, and 2.25 mm thick aluminum plate with one end screwed to a weighted (fixed) base. Holes were drilled on each side of the plate in 50 mm intervals to allow adjustment of the unsupported length of the beam. The PVDF strip was then affixed to the plate. Then, free-vibration was induced by manually displacing the free-end of the plate and then released. The generated voltage was collected using a Keysight InfiniiVision DSOX3024T oscilloscope. The voltage time histories were then processed using FFT in MATLAB, and the natural frequency of the system was identified.

Using this method of free-vibration response testing, the elastic modulus of each piezo-rod was determined. The different layers of the sensor system meant that they formed a composite structure. Therefore, the sensors' density and elastic modulus were estimated using the rule of mixtures in terms of volume fractions and known material properties. The density was determined to be ρ = 1,213 kg/m^3, and elastic modulus was ~ 3.0 GPa. For determining the moment of inertia, I, it was assumed that the acrylic rod was perfectly centered with the remaining space filled with marine epoxy (Fig. 4a). Due to differences in fabrication and epoxy cure, the elastic modulus was assessed individually for each sensor using free-vibration testing.

Hydrodynamic Testing

Flume test setup

The full length, width, and height of the flume used during hydrodynamic testing are 10, 0.6, and 0.7 m, respectively. In the center of the flume, there is a mobile bed zone

3 m long and 0.3 m tall that served as the test area. The mock pier and piezo-rods were installed in the mobile bed zone, which was filled with 0.3 m of sand. The sensors were driven into the sand surrounding the pier with the wires buried (Fig. 5).

In order to control speed of flow, the tail water board at the end of the flume can be adjusted to control water discharge. Consequently, a small angle between the tail water board and the flume yields a large discharge, and the opposite is also true. During the test, water was completely flushed and refilled prior to each set of tests for maintaining water clarity. All of the piezo-rods' lead wires were routed to one side and over the lip of the flume, staying as close to the sidewall as possible so as not to interfere with flow. The wires were then connected to a National Instruments DAQ PXIe-1062 chassis and PXIe-8133 controller equipped with a PXIe-4303, 32-channel analog input module with 24-bit resolution and ±10 V measurement range (sampling rate: 300 Hz). DAQ control and data storage was controlled using a customized program in LabVIEW.

Scour experimental details

Scour experiments were performed using two different piers, namely, one with a circular cross-section and the other square. Installation of each sensor began with driving the piezo-rod into the soil manually, without removing sand from the test bed. The lead wires were routed to one side of the flume and buried in sand. In total, 11 piezo-rods were

(a) (b)

Figure 5. (a) Photo showing the circular pier with piezo-rods after installation but before flow began. (b) Photo showing the square pier with piezo-rods after their installation but before the flume was filled with water.

installed in similar layouts for both sets of tests (Fig. 6), assuming symmetry of the scour holes based on previous studies (Azhari & Loh 2017). The piezo-rods were spaced to minimize interference between adjacent sensors but also so that a majority of the expected scour zone was covered. Sensors were oriented so that the face of the PVDF strip was orthogonal to the general direction of flow. After installation, the tail water board was brought to its highest angle. Water was then pumped into the flume at a controlled rate to gradually increase the water level to its maximum. Filling the flume with water allowed loose topsoil (or sand) to be removed while also compacting the sand near the pier and piezo-rods. This condition then served as the initial condition for which subsequent scour tests were performed.

Each scour test was separated into three data collection periods. The sand in this flume scoured rapidly, so by controlling the approximate flow velocity, three levels of increasing scour were induced. These periods will be referred to as (1) Low Scour, (2) Medium Scour, and (3) High Scour. For each period, flow conditions were maintained until the scour hole ceased to evolve. The increase in scour was confirmed visually and recorded manually at each sensor location before proceeding to the next scour period. Generated voltage data from all piezo-rods were collected simultaneously and throughout the entire test using the NI DAQ system.

Velocity experimental procedure

The piezo-rods were also tested under different flow velocities to measure flow effects on outputted fundamental frequencies. The sand bed was smoothed out as much as possible to allow flow to remain smooth throughout the test bed area. Three sensors,

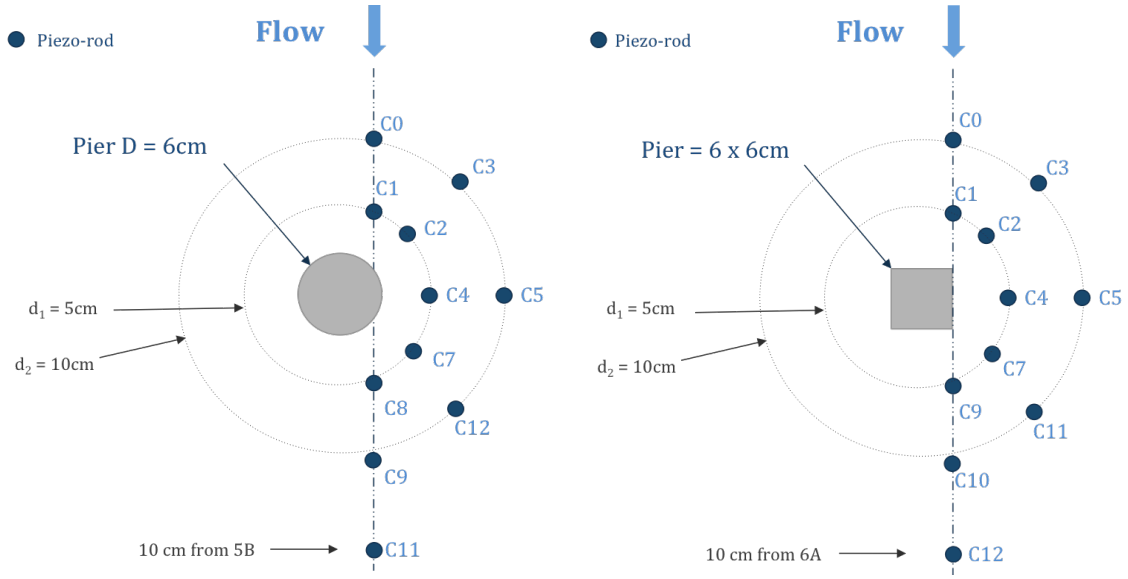

(a) (b)

Figure 6. These sensor layouts were chosen assuming symmetry in scour hole topography when flow is parallel to the main line of the sensor formation. (a) This schematic shows the location of piezo-rods installed around the circular pier (diameter: 6 cm). (b) Piezo-rod locations around the square pier (side length of 6 cm) are also shown. Each piezo-rod is labeled with the corresponding channel it was connected to during testing (*i.e.,* Channel 0 is marked as C0). Sensors were arranged along two concentric circles with diameters d_1 and d_2.

arranged in a row, were driven into the back portion of the mobile test bed and against the sandbox wall. A weighted plank was placed in front of the row of piezo-rods to prevent sediments from scouring away during the velocity test while also maintaining a fixed-end boundary condition. The flume was filled, and flow velocity was increased following the same procedure as mentioned earlier.

Results and Discussion

Calibration

The first set of tests involved conducting cantilevered free-vibration tests of the PVDF strip mounted on an aluminum plate in air. The unsupported length of the cantilever was varied from 0.3 to 1.05 m and in 0.05 m intervals. Figure 7a shows a representative time history voltage response of the aluminum plate (with an unsupported length of 0.4 m) undergoing free-vibration. This vibration testing was also performed on each of the developed piezo-rods in air to determine their elastic modulus. Processing the raw data using FFT resulted in its frequency response function (Fig. 7b). Figure 7c summarizes how the natural frequency varied as a function of length (or simulated scour depth). A calibration curve, where frequency was related to length, was determined using:

$$f = X * \frac{1}{L^2} \tag{11}$$

where, for the case of a fully fixed cantilever beam in air, the calibration coefficient X is:

$$X = \frac{1.876^2}{2\pi}\sqrt{\frac{EI}{\rho A}} \tag{12}$$

Using X, the corresponding elastic modulus could be calculated, especially since all other geometric parameters and density are known *a priori*.

The curve fitted to the raw data in Figure 7c was performed using a least-squares nonlinear fit line in MATLAB. For example, E as determined by curve fitting was ~ 63 GPa, which is consistent with the known properties of the cantilevered aluminum plate used for initial free vibration testing while considering influences from experimental error and an imperfect fixed boundary condition. Once the elastic modulus of the entire PVDF-and-aluminum cantilevered system is known, the length of the piezo-rod (or aluminum plate) can then be calculated for other test conditions, as shown in Figure 7d. It can be observed from Figure 7d that the calibration curve was able to predict the length of the sensor fairly accurately. These results confirmed that the PVDF sensing element could be extended using the proposed methodology and theoretically could be adjusted to whatever lengths needed for full-scale implementation. After the testing of multiple piezo-rods, it was found that the average elastic modulus, E, of 2.8 GPa was a more accurate estimation.

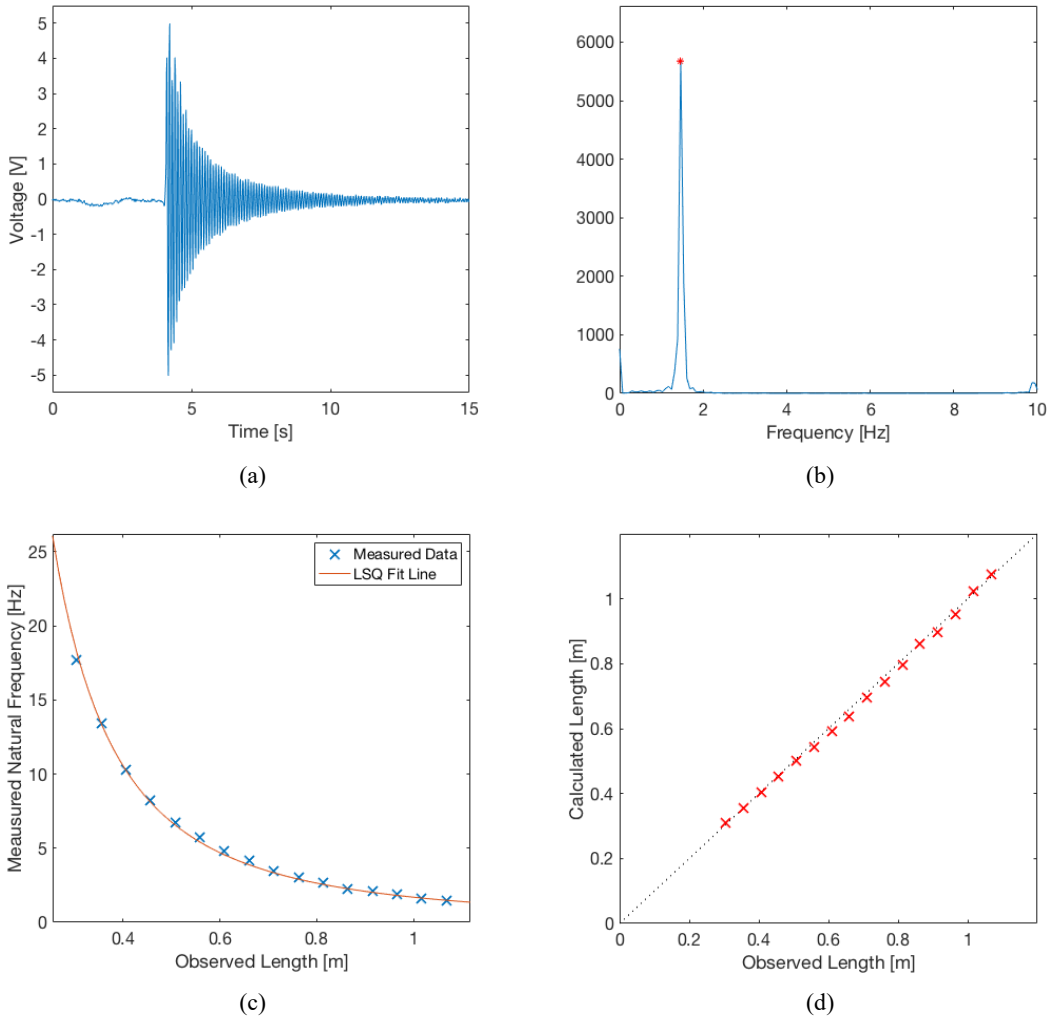

Figure 7. (a) Voltage output was collected from a sensor at 16 cm. (b) An FRF was used to make the fundamental frequency selection. (c) After determining the natural frequency at a set of length intervals, a LSQ fit line was used to estimate elastic modulus. (d) The lengths calculated from the estimated elastic modulus were plotted against the observed length during testing.

Scour experiments

Frequency domain analysis and filtering

Upon validating piezo-rod behavior in air, scour tests were performed using both circular and square piers. For each pier, three consecutive tests were performed to vary the severity of the scour hole, as was previously discussed. During each test, the sensors' lengths were recorded manually at the end of the Low, Medium, and High Scour periods. These lengths were used to produce scour topographies and to confirm deepening of the scour hole following each period (Fig. 8). These topographies also showed the presence of infill near the rear of the pier during both sets of tests.

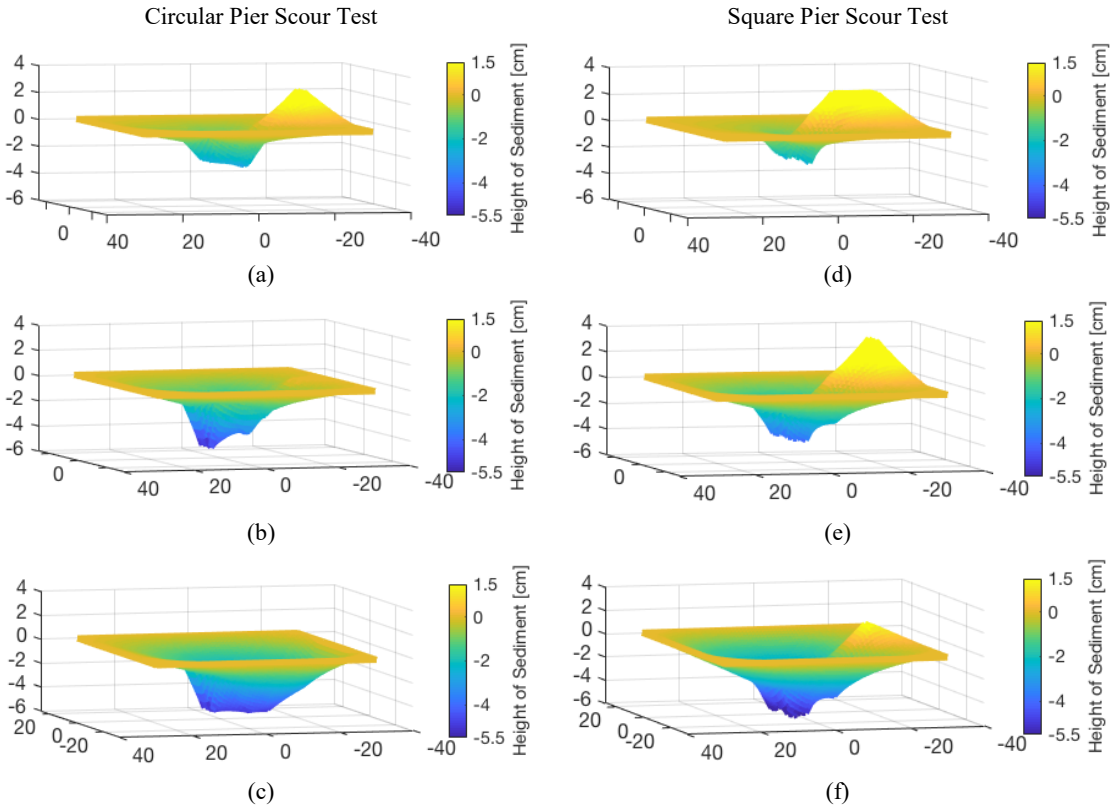

Fig 8. Manual measurements using the piezo-rod's tick marks and relative location in cm (Fig. 6) were used to produce topography plots during scour testing. (a) Low Scour during the circular pier test produced a relatively shallow hole and showed infill downstream of the pier. (b) Scour progresses during the circular pier Medium Scour period. (c) The final circular pier scour hole produced during High Scour was the deepest and had no infill. (d) Low Scour for the square pier produced a relatively shallow hole and shows substantial infill downstream of the pier. (e) Scour progressed during the Medium Scour period. (f) The final square pier scour hole produced during High Scour was the deepest and showed minimal infill.

The acquired voltage data from the piezo-rods were first smoothed using a moving average filter, and then a band-pass filter was applied to remove frequencies outside the range of 2 to 30 Hz. Data periods were then selected for analysis using windowing in the time domain, with each window being 10-s long and with 5-s of overlap with the previous window. Then, the PSD function for each window of data was computed, and a peak-picking algorithm identified the fundamental frequency. While most of the data analysis correctly identified the first mode of the piezo-rod, some datasets corresponded to times when the piezo-rod was only weakly excited.

Figures 9 and 10 show sample results from piezo-rods during the circular pier and square pier tests, respectively. Figures 9a and 10a show that piezo-rods undergoing large amounts of excitation were able to output their natural frequencies throughout the entire tests (*i.e.*, Low, Medium, and High Scour). These sensors, located upstream and to the side of the pier, typically showed higher voltage outputs than those downstream. Sensors on the side and downstream were observed to alternate between an in-line excitation plane (*i.e.*, orthogonal to the face of the PVDF element) and in the cross-flow direction. In many cases, downstream sensors favored vibration in plane with the face of the PVDF

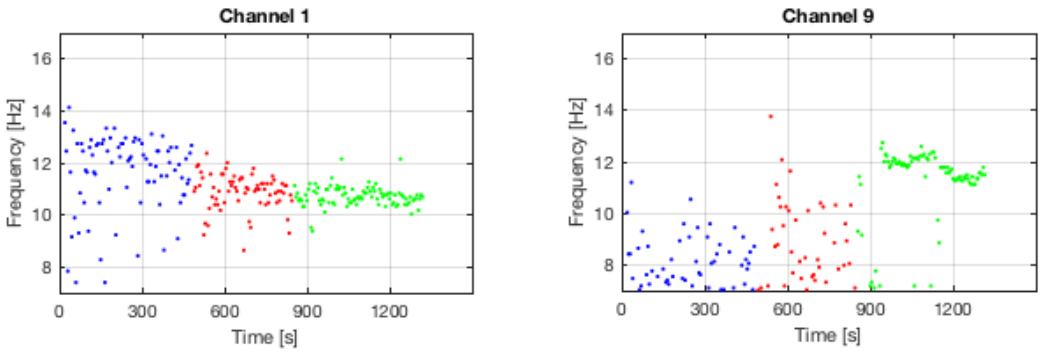

(a) (b)

Figure 9. Representative plots show the FFT outputted frequencies during the circular pier scour test. Each point represents the frequency output from a 10-s time window during the test. The blue section represents the Low Scour period, red represents Medium Scour, and green represents High Scour. Each flow period was consecutive, and the test was continuous, where flow was not stopped in between periods. (a) Channel 1, located upstream of the pier, showed good output with a clear trend during each scour period. (b) Channel 9, which was downstream of the pier, showed poor output due to low excitation until the High Scour period.

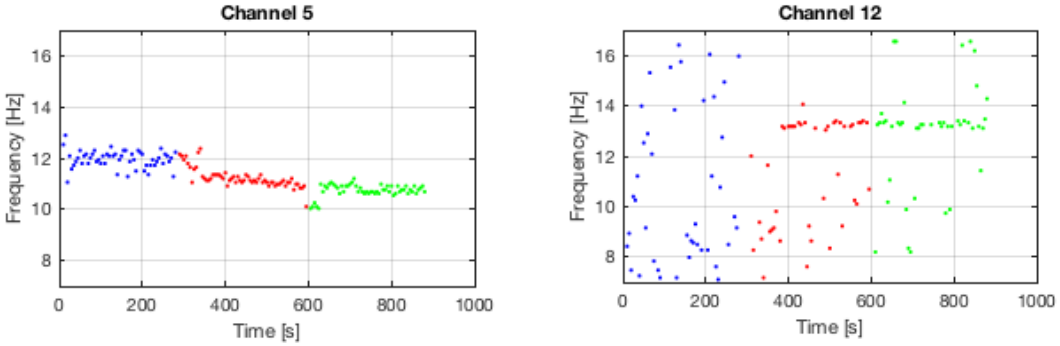

(a) (b)

Figure 10. Representative plots show the FFT outputted frequencies during the square pier scour test. Each point represents the frequency output from a 10-s time window during the test. The blue, red, and green sections correspond to the Low, Medium, and High Scour periods, respectively. Each flow period was consecutive, and the test was continuous, where flow was not stopped in between periods. (a) Channel 5, located to the side of the pier, showed good output with a clear decreasing trend with increasing scour. (b) Channel 12, which was downstream of the circular pier, did not produce reliable natural frequency measurements.

element, thereby causing very little discernible frequency output as seen in Figures 9b and 10b.

Overall, the topography of the scour hole deepened following the Low, Medium, and High Scour tests (Fig 8). In general, all channels with discernable data showed a corresponding downward trend in frequency as the sensors' length was further exposed. However, inconsistencies in fundamental frequency identification were observed on multiple channels, particularly those corresponding to sensors undergoing low amounts of excitation. Therefore, an alternative option for signal processing was sought.

Wavelet packet transformation and Hilbert transform

Based on the prominent frequency range found using FFT analysis, the decomposition levels for WPT were identified as 4 for the circular pier scour test and 3 for the square pier scour test. The time windows used were a total of 10-s with 5-s of

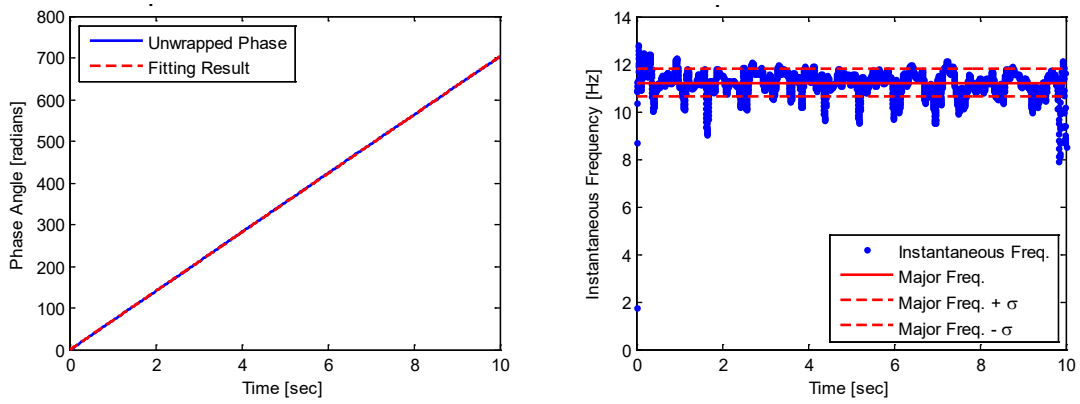

(a) (b)

Figure 11. (a) The phase function was calculated from the analytic function created by HT. (b) The instantaneous frequencies were obtained by differentiating the phase function. The major frequency was evaluated based on polynomial phase modeling

overlap. The windowed data was first decomposed by WPT to approach a narrowband condition. The frequency range for the first decomposed component in level 3 was from 0 to 18.75 Hz, and the frequency range for the first decomposed component in level 4 was from 9.38 to 18.75 Hz. HT eventually would have no practical meaning if the data occupied a wide bandwidth in the frequency domain, so decomposition levels were limited by the data's expected frequency range.

Then, HT was used to create the analytic functions, and the phase functions were unwrapped. This was followed by polynomial phase modeling to identify the major frequency. Figure 11 shows how the major frequencies were identified from the windowed data. This example shows Channel 6 in the square pier test during Medium Scour; every window throughout the duration of the test looked similar. A first order polynomial equation (Eq. 10) was adopted to fit the unwrapped phase functions, as shown in Figure 11a. The instantaneous frequencies were obtained by substituting the phase function into Equation 9. The standard deviation showed that the major frequencies were very close to the average of the instantaneous frequencies, as shown in Figure 11b. Consequently, the major frequency derived from polynomial phase modeling corresponds to the fundamental frequency of the piezo-rod sensor.

As shown in Figures 12 and 13, the two transforms not only successfully identified the fundamental frequencies, but they also showed a clearer, less scattered trend throughout each level of scour. For example, Channel 1 in both tests displayed a decreasing natural frequency trend, indicating that the piezo-rod was becoming more exposed due to increasing scour depth (as was also explained earlier). The natural frequency decreased from 13 to 11 Hz and from 11 to 9 Hz in the circular and square pier tests, respectively. This observation further confirmed that the piezo-rods could monitor scour depth under variable flow conditions. Notably, Channel 12 in the square pier test (Fig. 13) did not show an increasing trend moving from the Low to Medium Scour periods, in accordance with infill downstream during testing (Figs. 8d and 8e). However, after further review of this discrepancy, it was determined that Channel 12 experienced a

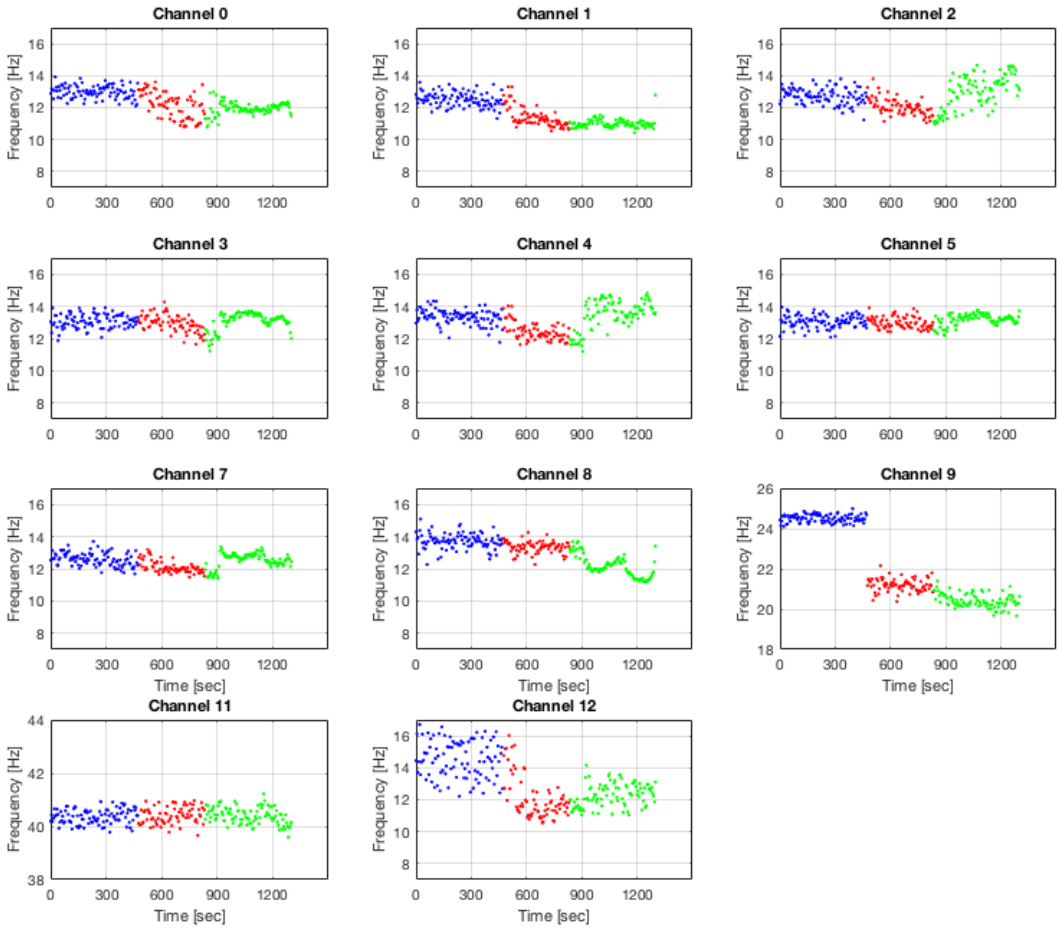

Figure 12. Plots show the WPT/HT outputted frequency from each time window during scour testing of the circular pier. The blue, red, and green sections represent the Low, Medium, and High Scour periods, respectively. Channels 6 and 10 were not used during the circular pier test.

fairly low signal-to-noise ratio, likely due to water infiltration, and underwent low amounts of vibration, so outputs from this channel should be disregarded.

Although a clearer trend could be extracted using the WPT and HT methods, some obscure results were observed during the circular pier test too (*e.g.*, Channels 2 and 12 in Fig. 12 and Channel 0 in Fig. 13). This resulted from dual frequency indicators in the decomposed component. The cause for this output was determined to be a dual resonance phenomenon, which occurs in long, slender cylinders. Such a bimodal response was captured due to a natural frequency occurring in each of the in-line and cross-flow directions (Sarpkaya 1995; Dahl et al. 2007). For Channel 2 in the circular pier test during High Scour, a biharmonic frequency condition, around 11.6 and 14.4 Hz, was seen during FFT analysis; however, in level 3, HT failed to distinguish the phase function. Therefore, decomposition to higher levels was used to separate frequencies on channels seen to have bimodal trends. After further decomposition (for instance, to level 6), the dual frequency could be separated, and a decreasing trend in natural frequency was found (Fig. 14). Similar decomposition could be performed on Channel 12 in the circular pier test and Channel 0 in the square pier test.

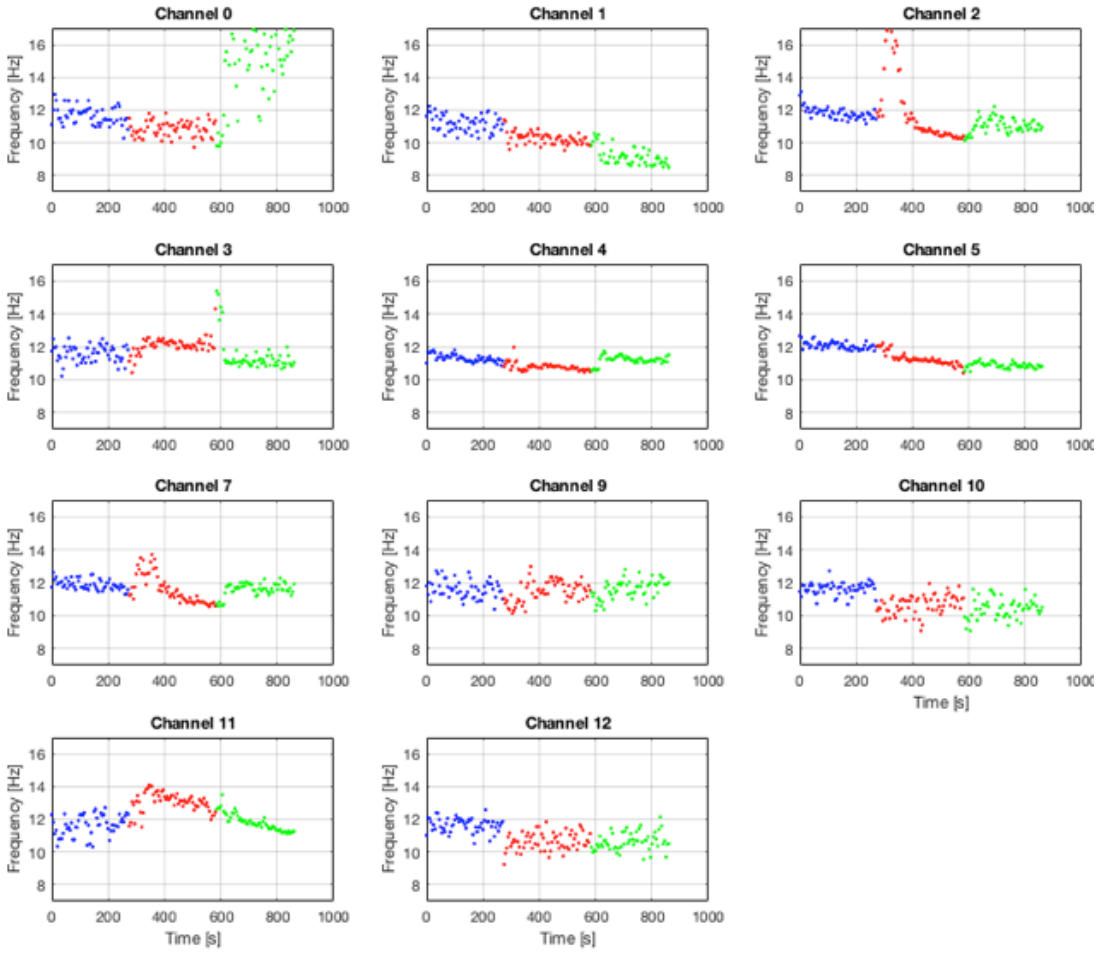

Figure 13. The plots show the WPT/HT outputted frequency from each time window during scour testing of the square pier. The blue, red, and green sections represent the Low, Medium, and High Scour periods, respectively. Channels 6 and 8 were not used during the square pier test.

After additional decompositions of these channels, the overall final result revealed a generally decreasing trend of natural frequencies as detected by each piezo-rod during each scour period. This result validated the ability of piezo-rods to detect very slight changes in their exposed lengths. As compared to conventional FFT analysis, the processing of the voltage time history data using WPT and HT is promising in that it allows a more discernable frequency trend to be extracted. WPT and HT also showed much better results when processing data collected during periods of low excitations, which are likely to present themselves in the field and during normal operations.

Velocity-frequency relationship

After processing the initial scour test data, upticks in frequency were noted at the beginning of each scour level, particularly during High Scour. This slight increase in natural frequency was attributed to one of two changing variables, namely, increase in velocity or decrease in scour depth. No notable infill was observed around the sensors in these periods during the scour test, so the piezo-rods' natural frequencies were tested for

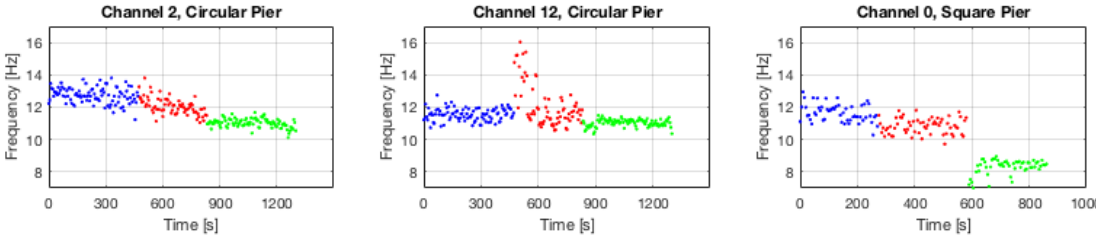

Figure 14. The plots show the WPT/HT outputted frequency on channels with dual frequency indicators after further decomposition.

flow velocity dependence. Thus, a test was conducted by mounting piezo-rods in the flume as it was subjected to fluid flow excitations. It should be mentioned that the test followed the same fluid flow protocol employed during the Low, Medium, and High Scour tests; flow velocity was adjusted and increased with time as data was continuously being aggregated. The sensors were mounted in a way that the exposed length of each piezo-rod remained the same.

For the velocity test, each channel's voltage time history was processed using the *spectrogram* function in MATLAB, which uses FFT to produce time-frequency plots (Fig. 15). Windowing was performed using 4-s windows with 50% overlap. A smaller

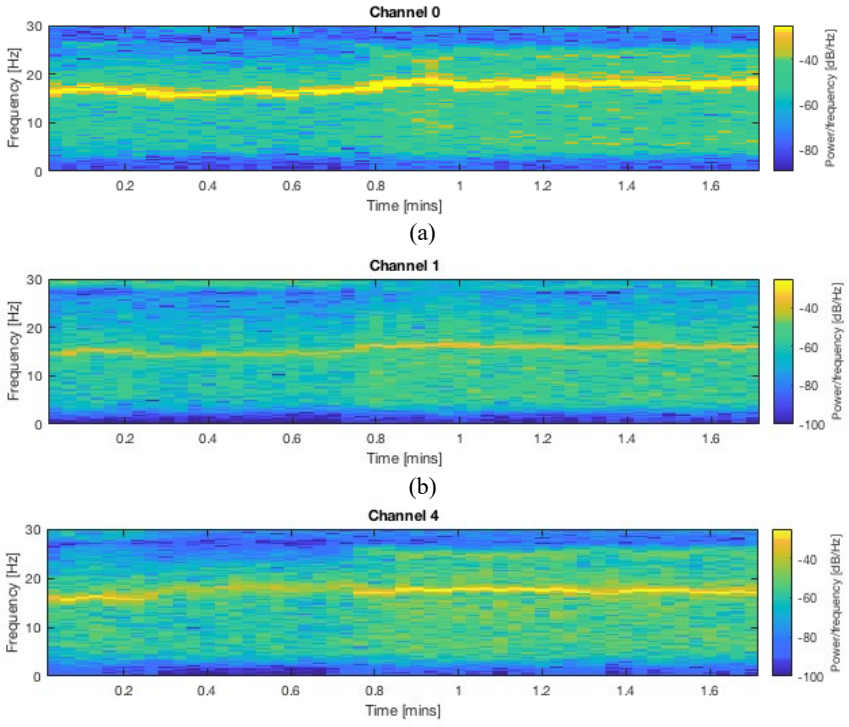

(a)

(b)

(c)

Figure 15. Time-frequency plots show the frequency spectra outputted during the velocity test. Each piezo-rod was kept at a constant length, and velocity was increased using the parameters from the Low, Medium and High Scour tests respectively. (a) The piezo rod connected to Channel 0 showed a clear output with a bump around 0.9 s. (b) The piezo-rod connected to Channel 1 showed a less clear response but sees its largest increase around 0.8 s. (c) The piezo-rod connected to Channel 4 shows a clear increase around 0.3 s and ends at a higher frequency than it began. All channels showed a 1 to 2 Hz increase in the major frequency.

time window was used due to the shorter duration of the test period. As seen in Figure 15, the time-frequency plot indicated a relationship between the flow velocity and the sensors' outputted fundamental frequency. As flow velocity increased, so did the natural frequency of the piezo-rod, which in this test remained fixed at a constant exposed length. The change in natural frequency due to overall velocity change for each channel did not exceed ~ 2 Hz, which is fairly small. This amount of natural frequency change matched well with the upticks seen in the frequency results (~ 1 or 2 Hz), particularly, at the beginning of the High Scour test, such as in Channels 0, 3, 4, 5, and 7 in Figure 12, as well as Channels 2, 3, 4 and 5 in Figure 13.

Discovery of this relationship goes against previous testing of an earlier generation piezo-rod (Azhari & Loh 2017). However, for long, slender cylinders, a relationship is known to exist between the cylindrical structure's oscillation frequency and the excitation flow velocity, due to a reduced added mass condition at high flow (Vandiver 1993; Vikestad, Larsen & Vandiver, 1997). This effect is also most pronounced in cylinders where the mass per length of the cylinder is relatively close to the mass per length of the displaced fluid, such as in this case. It could be that the previous study by Azhari & Loh 2017 did not vary flow velocity significant enough to observe this velocity-dependent frequency relationship. In addition, the length of the sensors used in the earlier study was also shorter. Regardless, further investigation will need to be undertaken to better correlate outputted frequency with length (especially at full-scale implementation), including precise velocity measurements throughout scour testing.

Summary and Conclusions

Local scour is a phenomenon that puts many bridges at risk of damage and ultimately failure. Currently, monitoring systems recommended for deployment by the FHWA have various shortcomings that may underestimate the extent of scour damage. Few technologies are able to provide substantial measurement of the area surrounding a pier without requiring ideal clear water conditions, while others only provide simple feedback at a single point or at sparse locations. To address these limitations, the design of a flexible buried piezoelectric rod for scour monitoring was developed and improved. In particular, this study validated that the PVDF sensing element could be easily extended to accommodate different lengths of piezo-rods and can be ultimately used for full-scale implementation. A 3D-printed cone footing was also developed for more realistic installation of these sensors, where the entire system was then tested in a hydraulic flume.

Results from the flume tests showed that the piezo-rod could be driven by hand using a cone footing system while successfully providing scour depth feedback throughout the entire duration of scour testing. First, traditional signal processing techniques based on Fourier analysis was used to detect changes in fundamental frequency as the piezo-rods were subjected to Low, Medium, and High Scour events. The results showed that the natural frequencies of the piezo-rods could be determined, although this was more challenging during the Low Scour test when the fluid flow excitation was weak. In addition, certain channels also exhibited two modal frequencies.

In light of these findings, Wavelet packet decomposition along with the Hilbert transform were used to estimate instantaneous frequency, and the results were compared with Fourier analysis results. It was found that WPT and HT could extract more points of frequency data from the same voltage time histories. Furthermore, clearer and less scattered frequency outputs were identified more consistently. Overall, this study presented a set of new analytical tools for extracting piezo-rod natural frequencies (and equivalently their exposed lengths or scour depth at their instrumentation locations). Future studies will focus on optimizing sensor design for different soil conditions and more complex flow environments, including more precise correlation of flow velocity with changes in natural frequency. More work is also needed to develop and test a full-scale implementation of the piezo-rod.

Acknowledgments

The authors gratefully acknowledge the Department of Civil Engineering, National Taiwan University for allowing the use of their hydraulic flume (Director: Prof. H. Capart). The authors also thank Mr. Honglei Lin for his assistance with data processing (University of California-San Diego) and Mr. Wei-Jay Ni (National Taiwan University) for his expertise and guidance with using flume. Furthermore, special thanks go to Ms. Tsai-Jung Kuo, Mr. Chuan-Fu Li, Ms. Yu-Xin Wu, and Mr. I-No Yu (all from National Taiwan University) for their assistance with running the scour tests and for collecting data during the experiments. This project was also conducted in collaboration with Prof. Michael Todd (UC San Diego) and Dr. A. Drew Barnett and Joseph Reed from Elintrix (Escondido, CA).

Funding

This research was supported by the U.S. Army Corps of Engineers (USACE) Cooperative Research Agreement No. W912HZ-17-2-0024.

References

Azhari, F. and Loh, K.J., 2017. Laboratory validation of buried piezoelectric scour sensing rods. *Structural Control and Health Monitoring*, *24*(9), p.e1969.

Azhari, F., Scheel, P.J. and Loh, K.J., 2015. Monitoring bridge scour using dissolved oxygen probes. *Structural Monitoring and Maintenance*, *2*(2), pp.145-164.

Bao, T. and Liu, Z., 2017. Vibration-based bridge scour detection: A review. *Structural Control and Health Monitoring*, *24*(7), p.e1937.

Boashash, B. and Jones, G., 1992. Instantaneous frequency and time-frequency distributions. *Longman Cheshire*.

Boashash, B., 1992. Estimating and interpreting the instantaneous frequency of a signal. II. Algorithms and applications. *Proceedings of the IEEE*, *80*(4), pp.540-568.

Boashash, B., O'Shea, P. and Arnold, M.J., 1990, November. Algorithms for instantaneous frequency estimation: A comparative study. In *Advanced Signal Processing Algorithms, Architectures, and Implementations* (Vol. 1348, pp. 126-149). International Society for Optics and Photonics.

Chen, G., Schafer, B.P., Lin, Z., Huang, Y., Suaznabar, O., Shen, J. and Kerenyi, K., 2015. Maximum scour depth based on magnetic field change in smart rocks for foundation stability evaluation of bridges. *Structural Health Monitoring*, *14*(1), pp.86-99.

Chen, S.S., Wambsganss, M.T. and Jendrzejczyk, J.A., 1976. Added mass and damping of a vibrating rod in confined viscous fluids. *Journal of Applied Mechanics*, *43*(2), pp.325-329.

Chen, Ssu-Ying, Yi-Jie Hsieh, Chih-Chyau Yang, Chien-Ming Wu, and Chun-Ming Huang. "A real-time bridge scour sensor system with accelerometers." In *Instrumentation and Measurement Technology Conference Proceedings (I2MTC), 2016 IEEE International*, pp. 1-6. IEEE, 2016.

Dahl, J.M., Hover, F.S., Triantafyllou, M.S., Dong, S. and Karniadakis, G.E., 2007. Resonant vibrations of bluff bodies cause multivortex shedding and high frequency forces. *Physical review letters*, *99*(14), p.144503.

De Falco, F. and Mele, R., 2002. The monitoring of bridges for scour by sonar and sedimetri. *NDT & E International*, *35*(2), pp.117-123.

Hunt, B. E., 2009. Monitoring Scour Critical Bridges*. Washington, D.C. Transportation Research Board*.

Johansson, M. 1999. *The Hilbert transform*. Mathematics Master's Thesis. Växjö University, Sweden.

Kong, X., Ho, S.C.M., Song, G. and Cai, C.S., 2017. Scour Monitoring System Using Fiber Bragg Grating Sensors and Water-Swellable Polymers. *Journal of Bridge Engineering, 22(7),* p.04017029.

Lagasse, P.F., Nordin, C.F., Schall, J.D. and Sabol, G.V., 1991. Scour monitoring devices for bridges. *Transportation Research Record,* (1290).

Lin, Y.B., Chen, J.C., Chang, K.C., Chern, J.C. and Lai, J.S., 2005. Real-time monitoring of local scour by using fiber Bragg grating sensors. *Smart materials and structures, 14(4)*, p.664.

Meirovitch, L., 1967. *Analytical methods in vibrations* (Vol. 438). New York: Macmillan.

Melville, B.W., 1975. *Local scour at bridge sites* (Doctoral dissertation, ResearchSpace@ Auckland).

Montalvo, C. and Cook, W., 2017. A Retrospective Analysis of Hydraulic Bridge Collapse. In *Congress on Technical Advancement* 2017 (pp. 22-28).

Richardson, E. V., 1989. *Bridge scour. Groundwater Data Collection. Series 4: Printed materials; Subseries 1: Materials by Richardson. Finding aid: http://lib.colostate.edu/archives/findingaids/water/wevr.html*.

Richardson, J.R., Price, G.R., Richardson, E.V. and Lagasse, P.F., OWEN AYRES & ASSOCIATES Inc and RESOURCE CONSULTANTS & ENGINEERS Inc, 1996. *Modular magnetic scour monitoring device and method for using the same*. U.S. Patent 5,532,687.

Sarpkaya, T., 1995. Hydrodynamic damping, flow-induced oscillations, and biharmonic response. *Journal of offshore Mechanics and Arctic engineering*, *117*(4), pp.232-238.

Stein, S.M., Young, G.K., Trent, R.E. and Pearson, D.R., 1999. Prioritizing scour vulnerable bridges using risk. *Journal of Infrastructure Systems, 5(3)*, pp.95-101.

U.S. Department of Transportation, Federal Highway Administration, 2005. *Field Observations and Evaluation of Streambed Scour at Bridges* (Publication No. FHWA-RD-03-052).

U.S. Department of Transportation, Federal Highway Administration, 2009. *Bridge Scour and Stream Instability Countermeasures: Experience, Selection, and Design Guidance, Third Edition* (Publication No. FHWA-NHI-09-111).

Van der Pol, B., 1946. The fundamental principles of frequency modulation. *Journal of the Institution of Electrical Engineers-Part III: Radio and Communication Engineering*, *93*(23), pp.153-158.

Vandiver, J.K., 1993. Dimensionless parameters important to the prediction of vortex-induced vibration of long, flexible cylinders in ocean currents. *Journal of Fluids and Structures*, *7*(5), pp.423-455.

Vaseghi, S.V., 2008. *Advanced digital signal processing and noise reduction*. John Wiley & Sons.

Vikestad, K., Larsen, C.M. and Vandiver, J.K., 1997. Experimental study of excited circular cylinder in current. In *Proceedings Of The International Conference On*

Offshore Mechanics And Arctic Engineering (Pp. 231-240). American Society Of Mechanical Engineers.

Wang, C.Y., Wang, H.L. and Ho, C.C., 2012. A piezoelectric film type scour monitoring system for bridge pier. *Advances in structural engineering, 15(6)*, pp.897-905.

Wickerhauser, M.V., 1996. *Adapted wavelet analysis: from theory to software*. AK Peters/CRC Press.

Yankielun, N.E. and Zabilansky, L., 1999. Laboratory investigation of time-domain reflectometry system for monitoring bridge scour. *Journal of Hydraulic engineering,* 125(12), pp.1279-1284.

Yao, C., Darby, C., Hurlebaus, S., Price, G.R., Sharma, H., Hunt, B.E., Yu, O.Y., Chang, K.A. and Briaud, J.L., 2010. Scour monitoring development for two bridges in Texas. In *Scour and Erosion* (pp. 958-967).

Zarafshan, A., Iranmanesh, A. and Ansari, F., 2011. Vibration-based method and sensor for monitoring of bridge scour. *Journal of bridge engineering,* 17(6), pp.829-838.